Journal Name

Dynamic Article Links ►

Cite this: DOI: 10.1039/c0xx00000x

www.rsc.org/xxxxxx

ARTICLE TYPE

NanoSIMS multi-element imaging reveals internalisation and nucleolar targeting for a highly-charged polynuclear platinum compound

Louise E. Wedlock,[a,b] Matt R. Kilburn,[b] Rong Liu,[b] Jeremy A. Shaw,[b] Susan J. Berners-Price*[a,c] and Nicholas P. Farrell*[d,a]

Received (in XXX, XXX) Xth XXXXXXXXX 20XX, Accepted Xth XXXXXXXXX 20XX

DOI: 10.1039/b000000x

Simultaneous multi-element imaging using NanoSIMS (nano-scale secondary ion mass spectrometry), exploiting the novel combination of ^{195}Pt and ^{15}N in platinum-am(m)ine antitumour drugs, provides information on the internalisation and subcellular localisation of both metal and ligands, and allows identification of ligand exchange.

Understanding the subcellular distribution of metal-based anticancer drugs provides key insights in identifying their organelle and molecular targets. Platinum-based chemotherapeutics have been the subject of intense investigation for decades due to the clinical success of cisplatin (Chart 1).[1] There have been numerous studies reporting the tagging of Pt complexes with fluorescent moieties to allow their intracellular distribution to be mapped using fluorescence microscopy,[2, 3] as well as various reports on the direct mapping of Pt inside tumour cells by using either synchrotron techniques[4] or electron microscopic methods.[5] Herein we report on the novel use of simultaneous direct multi-element imaging by nano-scale secondary ion mass spectrometry (NanoSIMS) to monitor tracking and distribution of ^{15}N-labelled Pt antitumour agents within cells. The results confirm the nucleolus as target of highly-charged polynuclear platinum drugs (PPCs), consistent with previous suggestions,[3] and show distinct differences in processing compared to the mononuclear agents.[6]

Significant advances have been made in visualising cellular distribution of metal-based therapeutics through the application of highly sensitive surface analysis techniques such as secondary ion mass spectrometry (SIMS), to cellular imaging.[7] SIMS has been used to study cisplatin-induced alterations in intracellular chemical composition in an established model (LLC-PK(1) cells) for studying renal injury.[8] Nano-scale secondary ion mass spectrometry, a recent development in SIMS instrumentation, combines exquisite spatial resolution (50 nm),

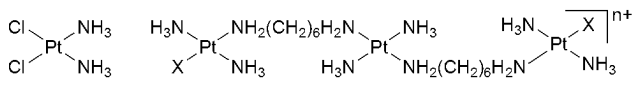

Chart 1 Structures of platinum antitumour compounds. Fully ^{15}N-labelled cisplatin and TriplatinNC were used in this study.

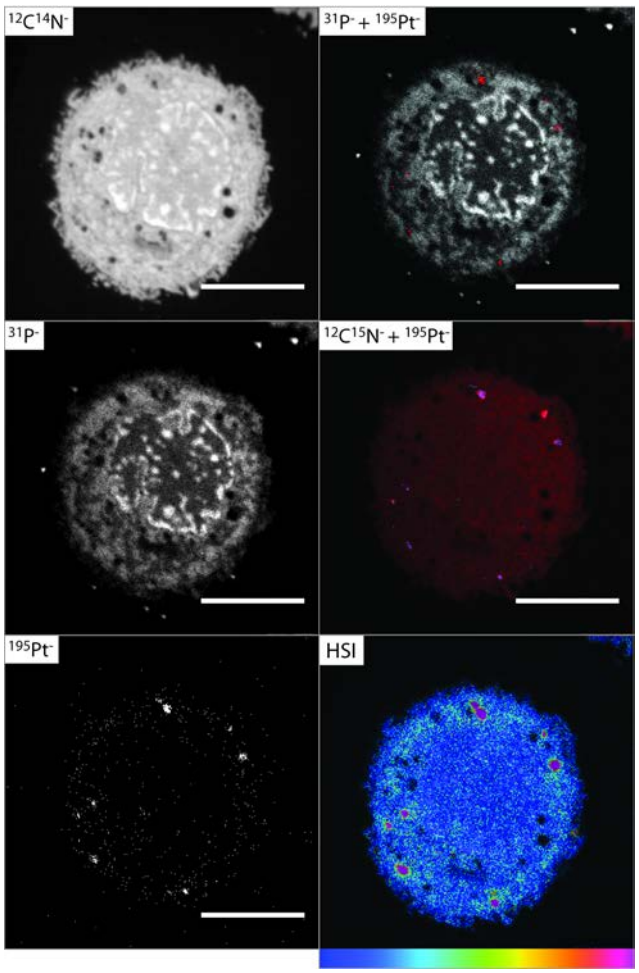

Fig. 1 Secondary ion maps acquired by NanoSIMS of fixed sections of an MCF7 cell treated with TriplatinNC (20 μM, 1 h). The $^{195}Pt^-$ (red) and + $^{31}P^-$ (greyscale) overlay shows no colocalisation of Pt and nucleic acids; the overlay of the $^{195}Pt^-$ (blue) $^{12}C^{15}N^-$ (red) secondary ion maps shows Pt and ^{15}N are mostly colocalised; the HSI representation of the $^{12}C^{15}N^-/^{12}C^{14}N^-$ ratio shows enrichment of ^{15}N in the cytoplasm as well as 'hotspots'; scale bars = 5 μm.

and the simultaneous detection of both heavy and light elements.[9] In NanoSIMS, a high-energy ion beam (Cs^+) is rastered across the sample surface, sputtering atoms from the topmost monolayers and generating negative secondary ions. The secondary ions are sorted according to their mass, producing a map of the sample

surface showing the distribution of the selected ion species. Furthermore, the high mass resolution of NanoSIMS allows the simultaneous detection of multiple isotopes of the same element (e.g $^{15}N/^{14}N$).[9] We have previously reported the use of NanoSIMS to detect Au inside tumour cells following treatment with an antitumour Au(I) phosphine complex, resulting in the identification of molecular targets not previously considered.[10] In this communication, we extend this technique to the dual imaging of both ^{15}N and ^{195}Pt inside cultured tumour cells following treatment with a ^{15}N-labelled polynuclear Pt compound, TriplatinNC, a non-covalent analogue of the Phase II clinical agent BBR3464 (Chart 1). The results are compared with similar treatment with ^{15}N-cisplatin.

Fig. 1 (and Fig. S1, ESI†) shows NanoSIMS secondary ion images of a fixed section of a single human breast adenocarcinoma (MCF7) cell after 1 h exposure to TriplatinNC (20 μM). The subcellular morphology, nucleic acid and Pt distribution are visible in remarkable detail, and the morphology of the cell is unchanged in comparison to untreated control cells (Fig. S2 and Fig. S3, ESI†). At this early time-point, the $^{195}Pt^-$ ion map shows a clear accumulation of Pt and the formation of discrete 'hotspots', possibly endocytic vesicle-like structures, close to the perimeter of the cell. An overlay of the $^{31}P^-$ and $^{195}Pt^-$ secondary ion images reveals conclusively that the Pt is not associated with DNA, where the falsely coloured red spots ($^{195}Pt^-$) are independent of the high $^{31}P^-$ signal. As the Pt compound was fully ^{15}N-labelled, both ^{14}N and ^{15}N counts were measured to determine regions where ^{15}N was present in an amount exceeding the natural abundance. The hue-saturation-intensity (HSI) image allows the direct visualisation of ^{15}N enrichment, where the value of the $^{15}N/^{14}N$ ratio is represented on a colour scale, and the intensity is an index of the statistical reliability.[9] The HSI image in Fig. 1 clearly shows enrichment of ^{15}N around the margin of the cell, and 'hotspots' in the cytoplasm (visible as pink).

The cellular accumulation of TriplatinNC (20 μM) was also examined after 2 h treatment. Significant accumulation of both $^{195}Pt^-$ and ^{15}N was observed; secondary ion images for two cells are shown in Fig. 2 (and Fig. S4, ESI†). In this case the Pt is located in the vesicle-like structures, and there is significant accumulation in the cytoplasm, reflecting greater accumulation with time. Notably, the HSI image shows ^{15}N enrichment in the nucleolus (grey arrow), at the exclusion of the nucleus. Similar to the cells treated with TriplatinNC for 1 h (Fig. 1), the overlay of the $^{12}C^{15}N^-$ (red) and the $^{195}Pt^-$ (blue) ion images in Fig. 2 shows that there is some colocalisation of ^{15}N and Pt after 2 h, however, interestingly, some of the regions of high Pt counts do not correspond to high enrichment of ^{15}N. This is more pronounced than at 1 h treatment, indicating some metabolism of TriplatinNC has occurred.

Secondary ion maps of fixed sections of single MCF7 cells treated with cisplatin under similar conditions (20 μM 1 h) were acquired and show that there are only very few Pt counts, the distribution of which is very diffuse (Fig. S5, ESI†), and that there is no detectable enrichment of ^{15}N (Fig. S6, ESI†). These results show that the uptake of TriplatinNC is significantly different to that of cisplatin and mononuclear cisplatin analogues, where uptake is slower and localisation indiscriminate.[6]

The ^{15}N enrichment was determined for whole cells and the individual subcellular compartments by extracting the data from the images, and is shown in Fig. S7 (ESI†), along with comparison to equivalent regions from the untreated control samples. These quantitative data support the observation of ^{15}N enrichment in the nucleolus of the cells, but also indicate a small enrichment within the nucleus. The nucleoli of cells treated with TriplatinNC for 2h were found to be enriched up to 0.423 ±0.002 at%, compared to the mean control value of 0.381 ±0.002 at%, while the surrounding nucleus was enriched up to 0.395 ±0.001 at%. The ^{15}N 'hotspots' are enriched by as much as 3.16 ±0.03 at% after 2 h. No ^{15}N enrichment was detectable for whole cells or subcellular compartments for cells treated with cisplatin under similar conditions (20 μM for up to 2 h), again reiterating the different uptake mechanism for the polynuclear Pt compound. The enrichment of ^{15}N in the nucleoli of the cells treated with TriplatinNC, in comparison to the surrounding nuclear regions, is demonstrated clearly by the plot in Fig. S7 (ESI†), and the localisation of ^{195}Pt in the nucleolus suggests that a targeting mechanism is responsible. These results confirm what has been seen previously using a fluorophore-TriplatinNC conjugate inside

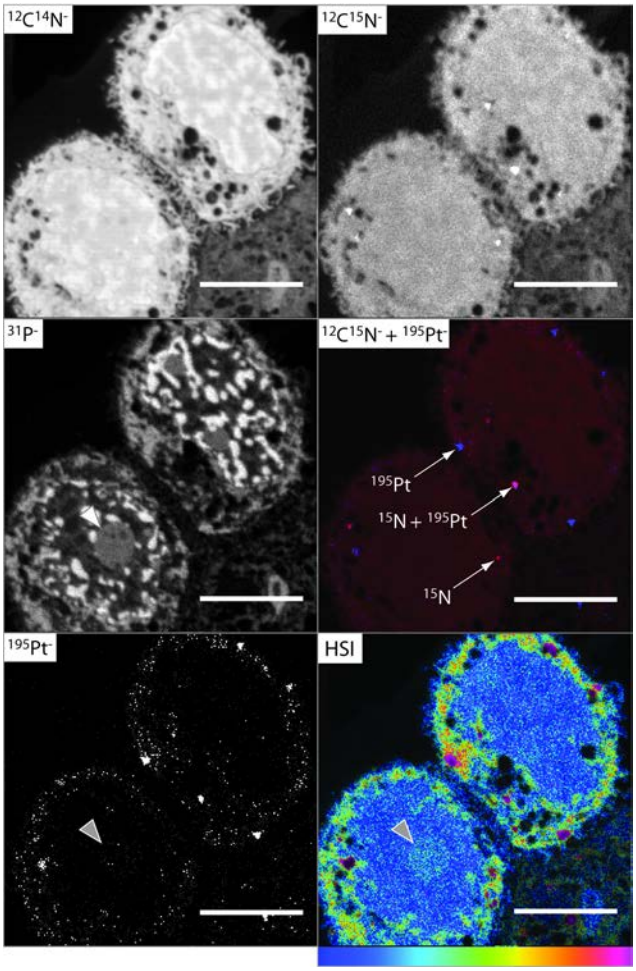

Fig. 2 Secondary ion maps acquired by NanoSIMS of fixed sections of an MCF7 cell treated with TriplatinNC (20 μM, 2 h). The $^{195}Pt^-$ secondary ion map and the hue-saturation-intensity (HSI) representation of the $^{12}C^{15}N^-/^{12}C^{14}N^-$ ratio map, clearly show localisation of both ^{195}Pt and ^{15}N within the nucleolus (grey arrow); the overlay of the $^{195}Pt^-$ (blue) $^{12}C^{15}N^-$ (red) secondary ion maps shows Pt and ^{15}N are colocalised in some but not all instances; scale bars = 5 μm.

HCT116 cells after 4 h, where the fluorescence originating from the conjugate was localised to the nucleolus and cytoplasm of the cells, with the exclusion of nuclear accumulation.[11]

The previous application of [^{1}H, ^{15}N] HSQC NMR methods has afforded significant insights into the hydrolysis and kinetics of DNA adduct formation of Pt drugs.[12] In a novel extension of this isotopic labelling technique, we have shown that multi-element mapping of Pt-am(m)ine antitumour drugs by NanoSIMS provides a significant contribution to metal-based therapeutics imaging, given that the drugs can be studied in absence of fluorescent labels, which can potentially influence pharmacokinetics of the "parent" structure. Moreover, localisation to specific organelles can be studied without the need for colocalisation studies employing specific markers, such as Fibrillarin as a nucleolar marker. Clear differences in localisation and time-course between cisplatin and the polynuclear Pt drug TriplatinNC are readily apparent. It is notable that the cellular accumulation of polynuclear, but not mononuclear, Pt is mediated through Heparan Sulfate Proteo Glycan (HSPG) interactions,[13] and the future use of NanoSIMS may contribute to understanding the internalisation of TriplatinNC upon HSPG binding. The identification of the nucleolus as a target for TriplatinNC confirms previous suggestions that this could be a novel target, with consequences for transcription inhibition.[3] Metabolism of the drug is also evident, as presumably ^{15}N in the absence of ^{195}Pt and *vice versa* (e.g. Fig. 2) indicates dissociation of the drug. Given that TriplatinNC is a "non-covalent" analogue of the Phase II drug BBR3464, further comparisons (including use of fully and partially (end or central NH_3 only) ^{15}N-labelled BBR3464), may delineate "noncovalent" contributions to the metabolic fate of the promising anticancer drug in exquisite detail, as well as expanding the intrinsically interesting properties of TriplatinNC itself.[1] Finally, simultaneous direct multi-element imaging by NanoSIMS is widely applicable to study of a wide range of other types of metal-based drugs, offering the exciting potential, demonstrated here, to probe ligand exchange reactions within intracellular compartments.

This work was supported by the Australian Research Council (Discovery grant to S.J.B-P and NF), and the National Institutes of Health (RO1-CA78754). We thank Erica Peterson and Luis Filgueira for helpful discussions and Ralph Kipping for synthesis and supply of ^{15}N-TriplatinNC. The authors acknowledge the scientific and technical assistance of the Australian Microscopy & Microanalysis Research Facility at the Centre for Microscopy, Characterisation & Analysis, The University of Western Australia, a facility funded by the University, State and Commonwealth Governments.

[a]*Institute for Glycomics, Griffith University, Gold Coast Campus, QLD 4222, Australia. Tel: +61 7 3735 7290, E-mail: s.berners-price@griffith.edu.au*
[b]*Centre for Microscopy, Characterisation and Analysis, The University of Western Australia, Crawley, WA 6009, Australia.*
[c] *School of Chemistry and Biochemistry, University of Western Australia, 35 Stirling Highway, Crawley, WA 6009, Australia.*
[d]*Department of Chemistry, Virginia Commonwealth University Richmond, Virginia, 23284-2006 USA. E-mail: npfarrell@vcu.edu.*

† Electronic Supplementary Information (ESI) available: Selected NanoSIMS data, cell culture and sample preparation methods, high mass resolution scans and image acquisition and processing details. See DOI: 10.1039/b000000x/

1. N. P. Farrell, *Drugs of the Future*, 2012, **37**, 795-806.
2. J. J. Wilson and S. J. Lippard, *Inorg. Chim. Acta*, 2012, **389**, 77-84; B. A. J. Jansen, P. Wielaard, G. V. Kalayda, M. Ferrari, C. Molenaar, H. J. Tanke, J. Brouwer and J. Reedijk, *J. Biol. Inorg. Chem.*, 2004, **9**, 403-413; G. V. Kalayda, B. A. J. Jansen, C. Molenaar, P. Wielaard, H. J. Tanke and J. Reedijk, *J. Biol. Inorg. Chem.*, 2004, **9**, 414-422; G. V. Kalayda, B. A. J. Jansen, P. Wielaard, H. J. Tanke and J. Reedijk, *J. Biol. Inorg. Chem.*, 2005, **10**, 305-315; G. V. Kalayda, G. Zhang, T. Abraham, H. J. Tanke and J. Reedijk, *J. Med. Chem.*, 2005, **48**, 5191-5202; R. Safaei, K. Katano, B. J. Larson, G. Samimi, A. K. Holzer, W. Naerdemann, M. Tomioka, M. Goodman and S. B. Howell, *Clin. Cancer Res.*, 2005, **11**, 756-767; X.-J. Liang, D.-W. Shen, K. G. Chen, S. M. Wincovitch, S. H. Garfield and M. M. Gottesman, *J. Cell. Physiol.*, 2005, **202**, 635-641; J. Gao, Y.-G. Liu and R. A. Zingaro, *Chem. Res. Toxicol.*, 2009, **22**, 1705-1712; E. J. New, R. Duan, J. Z. Zhang and T. W. Hambley, *Dalton Trans.*, 2009, 3092-3101; E. J. New, C. Roche, R. Madawala, J. Z. Zhang and T. W. Hambley, *J. Inorg. Biochem.*, 2009, **103**, 1120-1125.
3. B. T. Bendetti, E. J. Peterson, P. Kabolizadeh, A. R. Martinez, R. Kipping and N. P. Farrell, *Mol. Pharm.*, 2011, **8**, 940-948.
4. R. J. Mauthe, E. Sideras-Haddad, K. W. Turteltaub and G. Bench, *J. Pharm. Biomed. Anal.*, 1998, **17**, 651-663; M. D. Hall, R. A. Alderden, M. Zhang, P. J. Beale, Z. Cai, B. Lai, A. P. J. Stampfl and T. W. Hambley, *J. Struct. Biol.*, 2006, **155**, 38-44; M. D. Hall, C. T. Dillon, M. Zhang, P. Beale, Z. Cai, B. Lai, A. P. J. Stampfl and T. W. Hambley, *J. Biol. Inorg. Chem.*, 2003, **8**, 726-732; S. Harada, S. Ehara, K. Ishii, H. Yamazaki, S. Matsuyama, T. Sato, S. Oikawa, T. Kamiya, K. Arakawa, W. Yokota, K. Sera and J. Ito, *Int. J. Radiat. Oncol.*, 2009, **75**, 455-462.
5. G. L. Beretta, S. C. Righetti, L. Lombardi, F. Zunino and P. Perego, *Ultrastruct. Pathol.*, 2002, **26**, 331-334; C. Meijera, M. J. A. van Luyn, E. F. Nienhuis, N. Blom, N. H. Mulder and E. G. E. de Vries, *Biochem. Pharmacol.*, 2001, **61**, 573-578; Z. Yang, L. M. Schumaker, M. J. Egorin, E. G. Zuhowski, Z. Guo and K. J. Cullen, *Clin. Cancer Res.*, 2006, **12**, 5817-5825.
6. M. D. Hall, M. Okabe, D.-W. Shen, X.-J. Liang and M. M. Gottesman, *Annu. Rev. Pharmacol.*, 2008, **48**, 495-535; S. B. Howell, R. Safaei, C. A. Larson and M. J. Sailor, *Mol. Pharmacol.*, 2010, **77**, 887-894.
7. J. S. Fletcher, *Analyst*, 2009, **134**, 2204-2215.
8. S. Chandra, *Methods Mol. Biol.*, 2010, **656**, 113-130.
9. C. P. Lechene, F. Hillion., G. McMahon, D. Benson, A. M. Kleinfeld, J. P. Kampf, D. L. Distel, Y. Luyten, J. Bonventre, D. Hentschel, K. M. Park, S. Ito, M. Schwartz, G. Benichou and G. Slodzian, *J. Biol.*, 2006, **5**:20.
10. L. E. Wedlock, M. R. Kilburn, J. B. Cliff, L. Filgueira, M. Saunders and S. J. Berners-Price, *Metallomics*, 2011, **3**, 917-925.
11. E. J. Peterson, V. R. Menon, P. Kabolizadeh, B. T. Benedetti, R. Kipping, J. J. Ryan, L. F. Povirk and N. P. Farrell, Unpublished work.
12. S. J. Berners-Price, L. Ronconi and P. J. Sadler, *Prog. Nucl. Magn. Reson. Spectrosc.*, 2006, **49**, 65-98.
13. H. Silva, F. Frezard, E. J. Peterson, P. Kabolizadeh, J. J. Ryan and N. P. Farrell, *Mol. Pharm.*, 2012, **9**, 1795-1802.